Astron. Astrophys. 325, 1213–1225 (1997)

ASTRONOMY
AND
ASTROPHYSICS

Magnetic reconnection driven by emergence of sheared magnetic field

B. Schmieder[1], **G. Aulanier**[1], **P. Démoulin**[1], **L. van Driel-Gesztelyi**[1,3], **T. Roudier**[2], **N. Nitta**[4], **and G. Cauzzi**[5]

[1] Observatoire de Paris, section Meudon, F-92195 Meudon Principal Cedex, Trance
[2] Observatoire du Pic du Midi, F-65200 Bagnères de Bigorre, France
[3] Konkoly Observatory, Budapcst, PL, H-1525 Hungary
[4] Lockheed Palo Alto Research Laboratory, Palo Alto, CA 94304, USA
[5] Osservatorio Astronomico di Capodimonte, via Moiariello 16, I-80131 Napoli, Italy

Received 20 December 1996 / Accepted 10 March 1997

Abstract. Recurrent subflares (Class C) were observed in the NOAA 7608 active region on 27 October 1993. From multi-wavelength observations (white-light, magnetic field, H-alpha, X-ray), obtained during a coordinated campaign between Pic du Midi and Yohkoh, it appears that these flares were double ribbon flares caused by new flux emergence. As the flare begins, the X-ray emission observed with Yohkoh/SXT is loop-shaped with the axis almost parallel to the magnetic inversion line, while during the flare development, X-ray loops appear at the location of the emerging flux. The extrapolation of the photospheric magnetic field in a linear force-free field configuration allows identification of the magnetic configuration given by the flares. The Hα flare ribbons are located at the intersections of the computed quasi-separatrice layers (QSLs) with the chromosphere. We show that the initial loop-shaped X-ray emission region is in fact formed by several smaller loops directed in a nearly orthogonal direction with their feet anchored close to or in the Hα ribbons. During the flare development there are X-ray loops which represent only one foot of open or largescale magnetic loops. For the studied flares the puzzling soft X-rays observations could only be understood with the help of Hα and magnetic data combined with a modeling of the coronal magnetic field. Further, from the deduced magnetic field topology, the width of the QSLs and our present knowledge of 3-D magnetic reconnection, we conclude that the flare was due to magnetic reconnection driven by emergence of sheared magnetic field impacting in the pre-existing coronal field.

Key words: Sun: activity – Sun: chromosphere – Sun: corona – Sun: flares – Sun: magnetic fields – Sun: X-rays, gamma rays

1. Introduction

Yohkoh/SXT observed many "compact" flares which have a simple loop appearance, with bright knots at their tops. Brighter pixels indicate the presence of higher temperature and higher density plasma and imply that the loop is not in pressure equilibrium (Doschek et al. 1995). Such configurations are difficult to model, especially if they last for extended time intervals. For large events like long duration flares (Schmieder et al. 1996a), the classical model of continuous reconnection based on the Kopp and Pneuman concept, and developed by, for example, Forbes and Malherbe (1986) and Forbes and Acton (1996), can provide a satisfactory explanation. For compact flares, reconnection could occur impulsively and produce the observed enhancements of plasma temperature, while evaporation could provide high plasma density at the loop tops. However, if the involved magnetic structure is an isolated single loop, it becomes difficult to explain how this type of reconnection sustains itself for long periods of time. One has also to keep in mind that for small flares both limited spatial resolution and projection effects can lead to misinterpretation.

To know exactly what kind of flare one is looking at, it is absolutely necessary to know the magnetic field configuration in the corona at the time of the flare. Since this cannot yet be obtained with direct measurements, one needs to infer it, using multi-wavelength observations at all atmospheric layers. Good overlays between X-ray loops, Hα structures and magnetic maps and, also, a fit of the extrapolated field lines with coronal and chromospheric features, represent very effective tools in order to derive the coronal magnetic configuration. This has been demonstrated, for example, in van Driel-Gesztelyi et al. (1996), and Mandrini et al. (1996), where a series of X bright point flares, related to a minor flux emergence in a declining active region, were shown to be due to macroscopic reconnection between the pre-existing magnetic fields and the new bipole.

In this paper, we utilise multi-wavelength data for studying recurrent flare events observed in the NOAA AR 7608 on Oct. 27, 1993 (Sect. 2). The white light and magnetic field maps show the emergence of new flux. The Multichannel Double Pass Spectrograph (MSDP) provides the dynamics of the events and points

Send offprint requests to: B. Schmieder

out the occurence of two recurrent two-ribbon flares. The comparison of the Hα observations with the Yohkoh/SXT images gives a diagnostic of the relationship between the chromospheric and the coronal events. The extrapolation of the magnetic field and the analysis of its connectivities by using the new method developed by Démoulin et al. (1997) permit the construction of model of the coronal field configuration of the flare region (Sect. 3). Four systems of loops, two arcades and two series of open field lines, were drawn and identified with the observations. This shows principally that the apparent single loop is in reality an arcade of X-ray loops anchored in two ribbons visible in Hα. The X-ray flare loops represent the arcade of reconnected field lines. Combining the analysis of multi-wavelength observations with a magnetic model, we describe, in Sect. 4, what we learn about the evolution of the flaring configuration and the flare itself.

2. Observations

We follow the evolution of NOAA 7608 (NO9E40 on Oct. 27, 1993), and its flare activity, using magnetograms taken at Mees Observatory (Hawaii) and at Kitt Peak, photospheric observations taken at Debrecen, Yohkoh/SXT partial frame images and full disk images, and Hα data of the MSDP at Pic du Midi (see Table 1). No subtantial radio emission was detected in Ondrejov. Radio bursts of type III have been reported by Izmiran. This could indicate the existence of open field lines involved in the flare (Ruždjak and Zlobec, 1994). Yohkoh HXT and HXS did not register any hard X-ray emission, neither BATSE, apparently because the signal was too weak.

2.1. Evolution of active region 7608

This region consists of a large bipolar facular region P1-N1 (Fig. 1) or enhanced network, as seen in the magnetic maps obtained with the NASA/NSO spectromagnetograph of Kitt Peak (Harrison et al. 1992) and with the Imaging Vector Magnetograph (Mickey et al. 1996). We observe a parasitic polarity (positive) corresponding to a small pore on white-light pictures, surrounded by negative network (see P2 and N2 in Fig. 2). This emerging flux persists for more than a day (Oct. 26 and 27). The general magnetic configuration lasted longer than individual pores, which are difficult to identify, even within a few hours, in the white light images of Debrecen and continuum images from Kitt Peak and Mees Observatories.

2.2. Chromospheric activity

Of the several homologous subflares in this region, we have observed two double-ribbon flares of class B2.8 at 09:15 UT and of class C1.0 at 11:30 UT (Fig. 3). The MSDP spectrograph allows us to obtain intensity and velocity maps in the Hα line at &, $\Delta\lambda = \pm 0.3$Å or± 0.6Å (Mein, 1977). We present the maps at $\Delta\lambda = \pm 0.3$Å (Figs. 5, 6 and 7c). The spatial resolution is about 0.5 arc sec. The dimension of an elementary field of view is 30 arc sec by 4 min. The observations show both dark regions and emission regions. The first ones correspond to filaments and/or Arch Filament System (AFS) above emerging flux (see for example Mein et al. 1996); the second ones are ribbons heated by deposited energy.

Table 1. Characteristics of the observations on October 27, 1993

Wavelength	Instruments	pixel size	time in UT
White Light	Debrecen	0.5 $''$	from Oct 25 to Oct 29
Hα	MSDP (Pic du Midi)	0.225 $''$	08:58-09:55, 10:38-12:01
Magnetic data	Mees (Hawaii)	1.2 $''$	17:46, 20:48
	Kitt Peak	1.0 $''$	17:22-18:15
X-ray	Yohkoh/SXT	2.46 $''$	05:40-06:40, 07:15-08:18, 08:52-09:55, 10:28-11:32

The structure of the bright regions is composed of two parallel ribbons, one following the curved shape of the negative polarity N1 and the other overlying the positive parasitic (included) polarity P2 (Fig. 4). They are on both sides of the magnetic inversion line. The morphology of the region does not seem to change drastically due to the flares since the flare ribbons are homologous in the two flares. Nevertheless, we observe some local changes in the orientation of Hα structures during the first event (09:15 UT, see Fig. 5 right pannels). In the pre-flare phase (09:08:00 UT) the filaments are nearly parallel to the magnetic inversion line between the polarities P2 and the northern part of N1, while after the flare (09:19:49 UT) the AFS is nearly perpendicular to the inversion line. The simplest interpretation of these observations is the following. Before the first flare, an emergence of sheared (or twisted) magnetic field took place (as reported in other cases by Leka et al. 1996). The magnetic free energy of the configuration is then released during the flare.

For the second flare (11:27:59 UT) in the preflare phase we observe a large blueshift corresponding to the rising AFS between N2 and P2 (Fig. 6 at 11:27:59). By the time of the flare at 11:29:18 UT the two ribbons are close to each other in a region between N1 and the eastern side of P2. Furthermore, an extension of the ribbon above the negative polarity toward the north-west part of N1 is detected with intense Hα emission which was not present in the previous flare. At the flaring time the ribbons show some maxima of intensity whose size is of the order of 5 by 10 pixels. They correspond to 1.2×2.3 arc sec kernels.

2.3. Flares

As seen in Fig. 3, Yohkoh fully observed the flare at 09.15 UT, and only the rising phase of the flare at 11:30 UT. The general appearance of the region in soft X-rays as observed with the soft X-ray telescope (SXT) aboard Yohkoh (Tsuneta et al. 1991) is shown in Figs. 1 and 7a. The first flare evolution is presented in Fig. 5 (left pannels). The co-alignment of X-ray images and

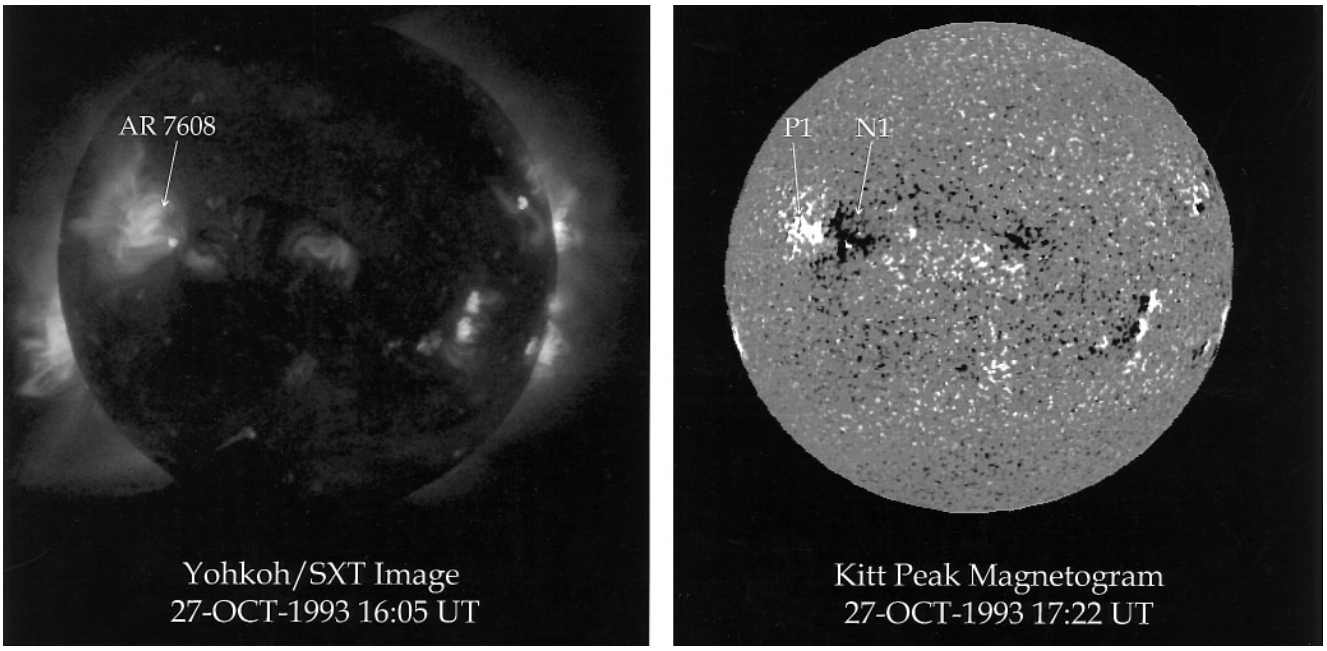

Fig. 1. Left: Full disk X-ray image observed with Yohkoh/SXT Right: Kitt Peak magnetogram of October 27, 1993. The two main polarities of the active region studied are indicated with the labels P1 and N1. North is up.

Table 2. Temperature and electron density in the C-shaped loop and in the flare kernel (maximum value) for the first flare and the eastward X-ray loop arcade for both of the flares (averaged values).

Region	Temperature 10^6K	EM cm^{-3}	area pixels	EM cm^{-5}	Diameter km	Ne cm^3
C-shaped loop	6	8 10^{47}	144	1.8 10^{29}	2000	1.1 10^{10}
flare kernel	7	3 10^{47}	23	5.0 10^{29}	2000	6.0 10^{10}
loop arcade	4	1.5 10^{46}	153	0.3 10^{28}	10 000	1.2 10^9
single long loop	4	1.5 10^{46}	63	0.8 10^{28}	10 000	3.0 10^9

magnetograms has been made by using Kitt Peak magnetogram and Yohkoh/SXT full disk image.

In the initial phase of both flares, the soft X-ray brightenings are located to the north-east of the parasitic polarity P2 (Fig. 4). For the 09:15 UT flare, the X-ray emission has a loop-like shape which overlays the magnetic inversion line and follows the Hα ribbon shape (see Fig. 5a and Sect. 2.4). We call this structure a "C-shaped X-ray loop". This morphological similarity between X-rays, Hα and the magnetic inversion line is puzzling with respect to a classical flare model, where the soft X-ray loops outline magnetic loops located at the border of Hα ribbons. The maximum intensity in X-ray overlays the Hα flare kernel (Fig. 5c). During the development of the flare, the X-ray emission shifts to the west (Fig. 5e). Small loop-like structures are present above the Arch Filament System. We call this structure a "fishbone X-ray loops"; it appears as an extension to the north-west of the previous C-shaped X-ray structure which is still present, although fainter. Like in the initial flare phase, the X-ray morphology is surprising with respect to other observations. In particular, why does the maximum emission shift position, and why should the fishbone X-rays loops occur just at the location of the emerging AFS?

At the north-east of the above described compact X-ray emission, large scale X-ray loops are observed with a nearly east-west direction (Fig. 7a), connecting N1 to P1. We call this structure an "arcade of X- ray loops". All of them end before reaching the compact emission region. This arcade of X-ray loops seem to be somewhat brightened by the repeated flarings between 03:00 UT and 11:00 UT. We cannot give more details of the evolution since there were relatively few full disk SXT images during this programme, only 9 composite linages.

Further to the north-east we have a series of diffuse X-rays loops (Figs. 1 and 7a). Particularly noticeable is the long northern loop, whose emission increases by a factor of 3 during the interval of 8 hours (03:00 UT and 11:00 UT) with an additional 10% brightening around the 09:15 UT flare. This may indicate a possible link between them and the flare. They start from P1 and close to the eastern part of AR 7608 where there is no clearly defined polarity on the Kitt Peak magnetogram (Fig. 1), probably because we are too close to the limb for magnetic detection of vertical fields. Like for the large scale X-ray loops

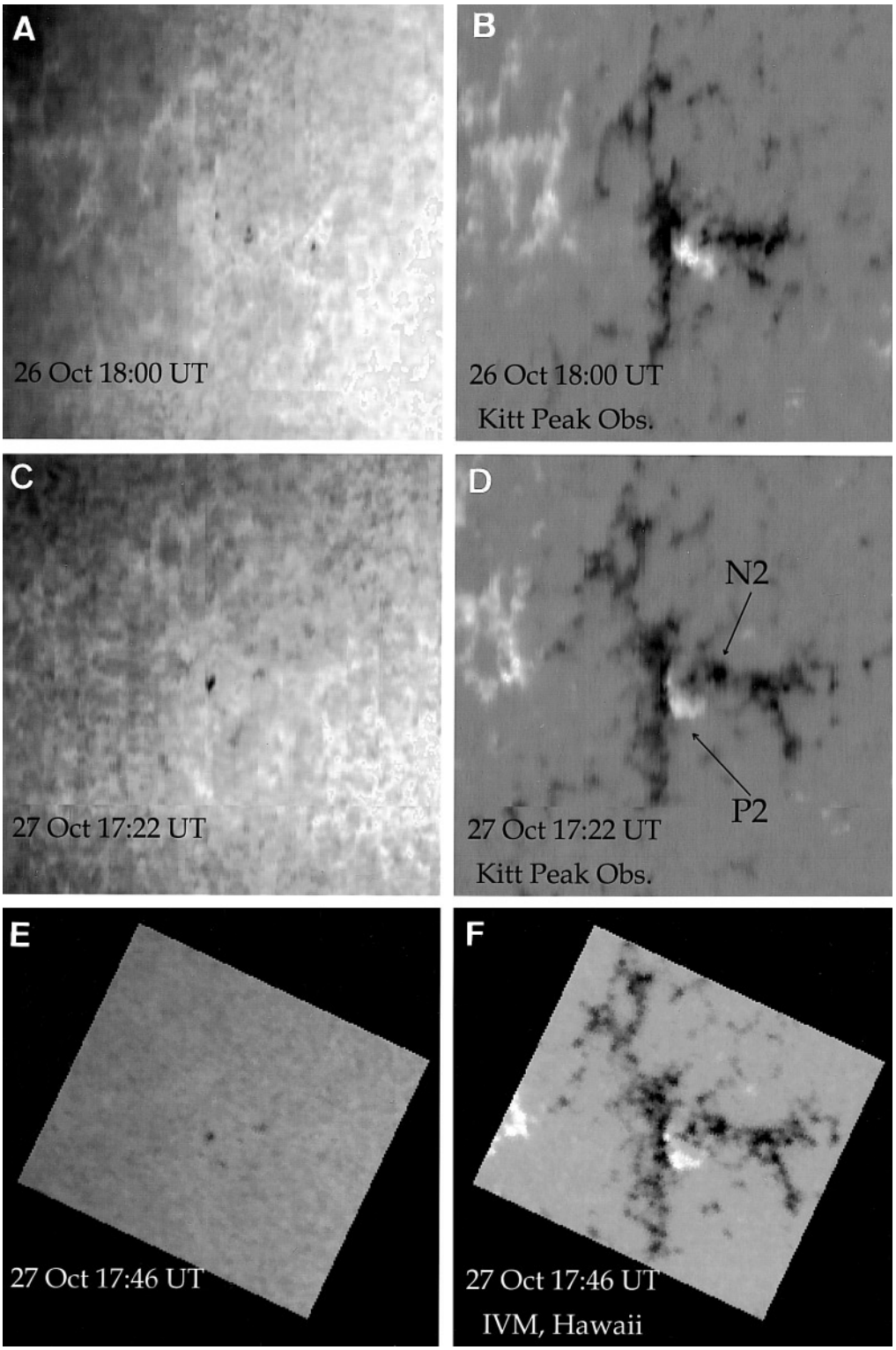

Fig. 2. a,c,e Continuum images and **b,d,f** magnetograms showing the time evolution of photospheric pores and magnetic features between Oct 26 and Oct 27, 1993. **a-d** are from Kitt Peak Observatory and **e-f** from Mees Observatory (Hawaii, Imaging Vector Magnetograph).

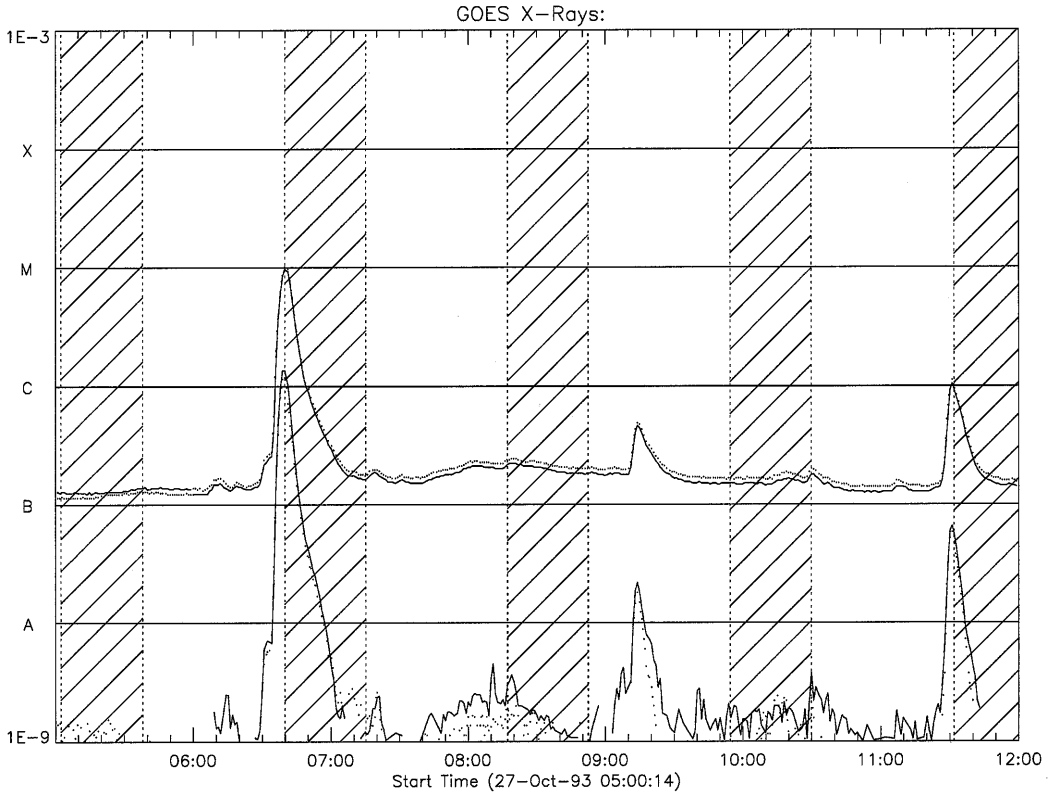

Fig. 3. GOES X-ray light-curves (two channels). Arrows indicate the studied flares and the striped regions show the nights of the Yohkoh satellite.

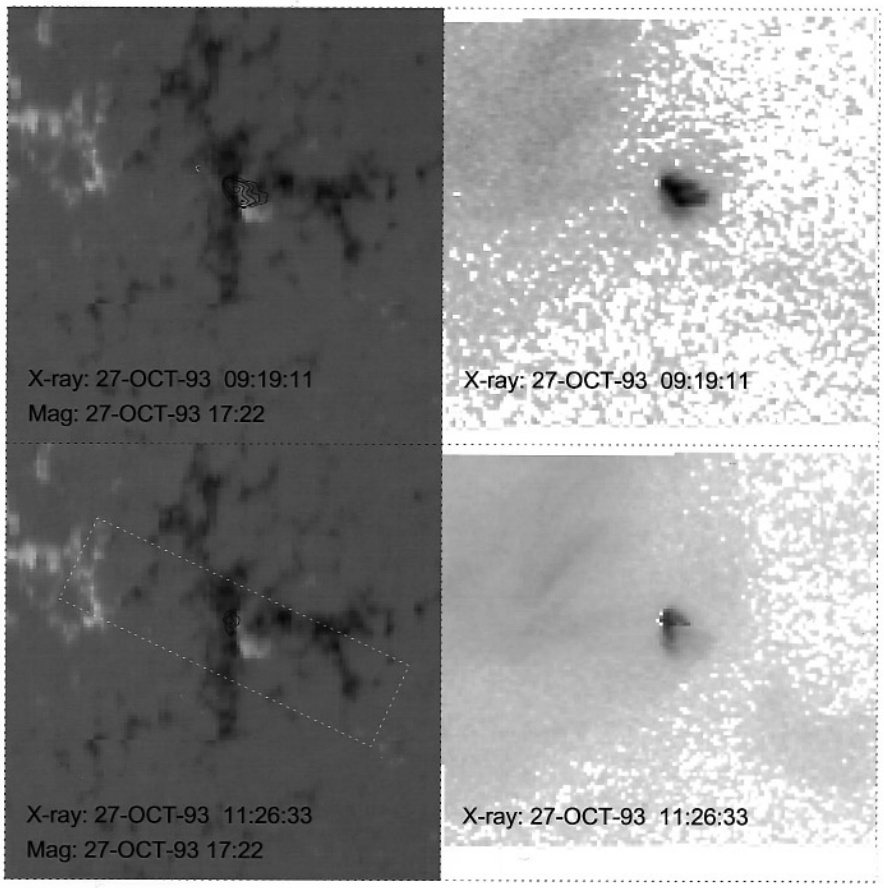

Fig. 4. Magnetograms of Kitt Peak with contours of X-rays superimposed and SXT images for the two homologus flares of 09:15 UT and 11:30 UT. Black/white correspond to negative/positive polarities. North is up. The long dashed box in the left bottom panel represents the field of view of the MSDP Hα spectrograph.

of the previous paragraph, there is no evidence of magnetic connection to the flaring region. Both sets of loops may have been excited by a sympathetic flaring process (linked to, MHD disturbances propagating from the flare site) (see Sect. 3.3).

2.4. Temperature and electron density

The soft X-ray Telescope provided partial frame images using alternatively thin Al 0.1 μm and thick Dagwood AlMg filters with a cadence of 17 sec. The sensitivity of the filters allows observations of material in a logarithmic temperature range between 6 to 7 with an accuracy of 0.1 (Hara et al. 1992). The image is 128 $\times$ 128 pixels with a pixel size of 2.46 arc sec (full resolution partial frame). To compute the temperature T and the emission measure EM as a function of time we used the *Yohkoh* software GO-TEEM. From the EM we computed the electron density assuming cylindrical geometry (Table 2).

The electron density is calculated in the flare loops only for the first flare, because the second was not fully observed by Yohkoh. An estimate of EM for the second flare was obtained using BCS (Schmieder et al. 1997a) and it is consistent with that measurcd for the first. In the flare loop region we have considered two areas defined by intensity contours: one concerns the whole envelope of X-ray emission (the "C-shaped loop"), and the second one the brightest part of the X flare loop (flare kernel). The indicated values of EM correspond to the flare time. If we take into account the number of pixels inside the contours and the pixel size 2.46 arc sec we obtain EM values per cm^{-5}. For both flares, electron density is calculated in the adjacent (eastward) arcade of loops. Two areas were also analysed, defined by contours: one concerns the whole envelope and one an individual loop. We obtained similar values of EM in the arcade of X-ray loops for both of the flares. These values are averaged over one hour around the flare time.

There is more than an order of magnitude difference in the electron density between the flare region and the adjacent loops (the flare density values are minimal values because the kernels are in fact smaller than the considered area, so that this ratio is expected to be even greater). These values are used in the modeling section.

Comparing X-rays and Hα observations we conclude that the compact X-ray emission with a loop shape is in fact the envelope of an arcade of loops joining the two ribbons with its axis following the curved inversion line of the magnetic field (Fig. 4). We confirm this assertion below by analysing the magnetic field line linkage in the region.

3. Model

Using the magnetic fields extrapolated from the photosphere, we locate the regions where reconnection can take place, using the quasi-separatrix layer method (see Démoulin et al. 1996). The computed QSLs compare favorably with the bright Hα ribbons, where the energy is released at the chromospheric level. Taking into account the observed horizontal motions wich slightly modify the magnetic configuration, we find that ideal MHD breaks down at the computed QSLs and that the flare is driven there by magnetic reconnection, between the field lines of the observed rising AFS and soine large pre-existing coronal loops.

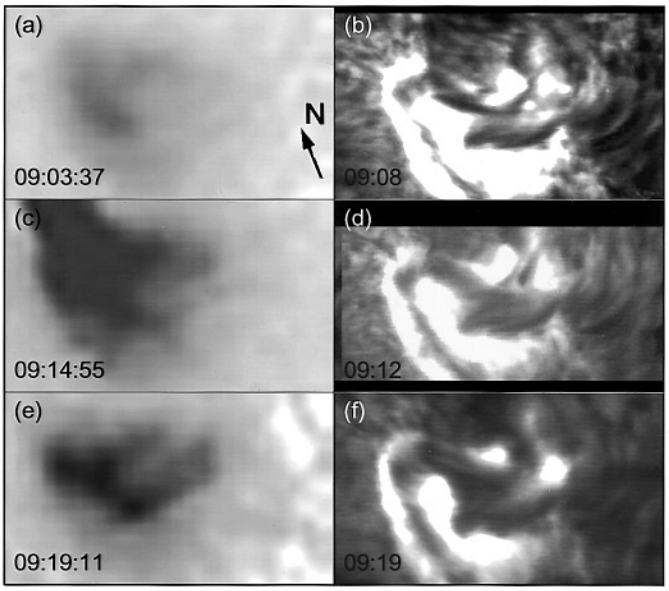

Fig. 5. Evolution of the 09:15 UT flare in X-rays (a,c,e) and Hα (b) at 09:08 UT, (d) at 09:12 UT, (f) at 09:18 UT. In (b) horizontal fibrils between the ribbons are identified as sheared filaments. The flare kernels correrpond to the X-ray saturated pixels (in c), note in pannels (a) and (c) the C-shaped X-ray loop and in (e) the fishbone structure. The X-ray images have been rotated to be co-aligned with the Hα images.

3.1. Extrapolation of the photospheric field

Using Kitt Peak magnetogram, we extrapolate the photospheric longitudinal field (B_l) of the entire active region to the corona. In order to do so, we assume that the force-free field assumption is satisfied. This gives:

$$\nabla \times \mathrm{B} = \alpha \mathrm{B} \tag{1}$$

We use the linear approximation, where α is a constant which gives a proportionality between the current density and the magnetic field. The extrapolation uses the fast Fourier transform, which imposes a periodicity of the solution in the horizontal (x, y) directions (Alissandrakis 1981). This numerical method is restricted to the study of active regions with low magnetic shear. The maximum shear that can be used is given by $\alpha_{\max} = 2\pi/L$, where L is the horizontal size of the computational box. With a greater shear, the large-scale harmonic solutions become periodic with height, implying an infinite energy in the field. These could be discarded, but it would change the boundary conditions. So we limit ourselves to $\alpha < \alpha_{\max}$.

Furthermore, we have to take into account the fact that the studied region AR 7608 is not at the center of the solar disk. So the longitudinal magnetic field, given by the magnetogram, is tilted towards the photosphere. This effect provides the appearance of parasitic magnetic polarities which are not real (see

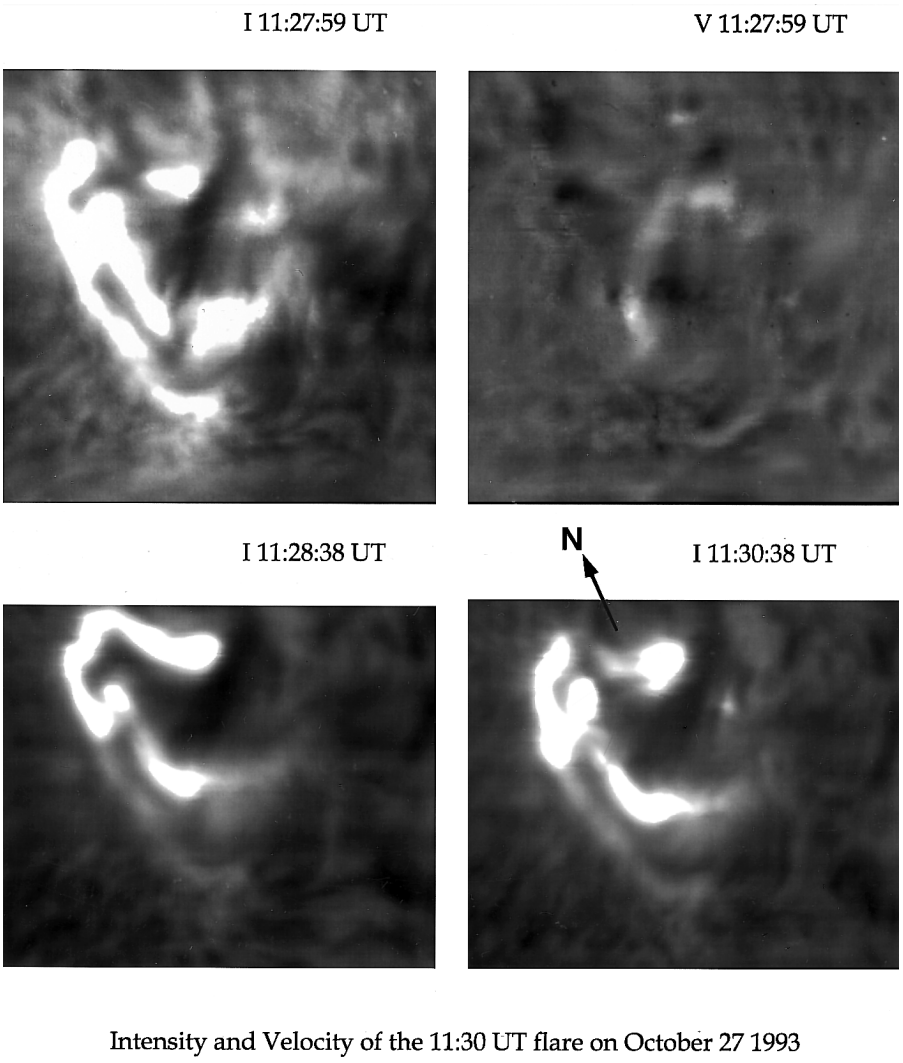

Fig. 6. Evolution of the two ribbon flare observed at Pic du Midi in Hα with the MSDP spectrograph at 11:30 UT: intensity and velocity maps (white/black corresponds to blue/redshift). Note the blueshift corresponding to the arch-filament system rise. The top panel dimension is 256 $\times$ 256 pixels, the low panel 256 $\times$ 215 pixels, the pixel size being 0.225 arc sec.

Démoulin et al. 1997). Which is why we have to get rid of the projection effects. Using a full vector magnetogram would eliminate this problem, unfortunately, Hawaii's data for the transversal component of the magnetic field are too noisy in this low field region, so we can not use them to compute the true vertical field. We rather assume that the magnetic field is vertical at the photospheric level where it is measured by Kitt Peak magnetogram. We simply reorientate the longitudinal measured field to a vertical position.

3.2. Quasi-separatrix layers method

Classical reconnection occurs at separatrices, where the field line linkage is discontinuous. On the other hand, it has been shown that ideal MHD can be broken in the presence of strong gradients in the field line linkage (Priest & Démoulin 1995). Though the magnetic topology does not show any discontinuity at such locations, the resistive term in Ohm's law can be enhanced when the plasma, which is initially frozen in the magnetic field, cannot follow the motion of the field lines. When they become super-Alfvénic, the field lines slip through the plasma, and reconnection may take place. These regions are called quasi-separatrix layers or QSLs.

They are characterized by their width and the value of the norm of the displacement gradient vector D. It is defined when mapping, by field lines, pointing from one section to another in the photosphere. We call its norm $N(X, Y)$ (x and y refering to the photospheric plane) and defined it as in Démoulin et al. (1996). A simplified view of QSLs is the following: Let us consider two field lines, 1 and 2, with their respective footpoints (A_1, B_1) and (A_2, B_2); in a QSL the distance between A_1 and A_2 is very different from the one from B_1 and B_2. For instance, a QSL will be important in flaring configurations if two field lines, that are initially close to one another (A_1 is close to A_2),

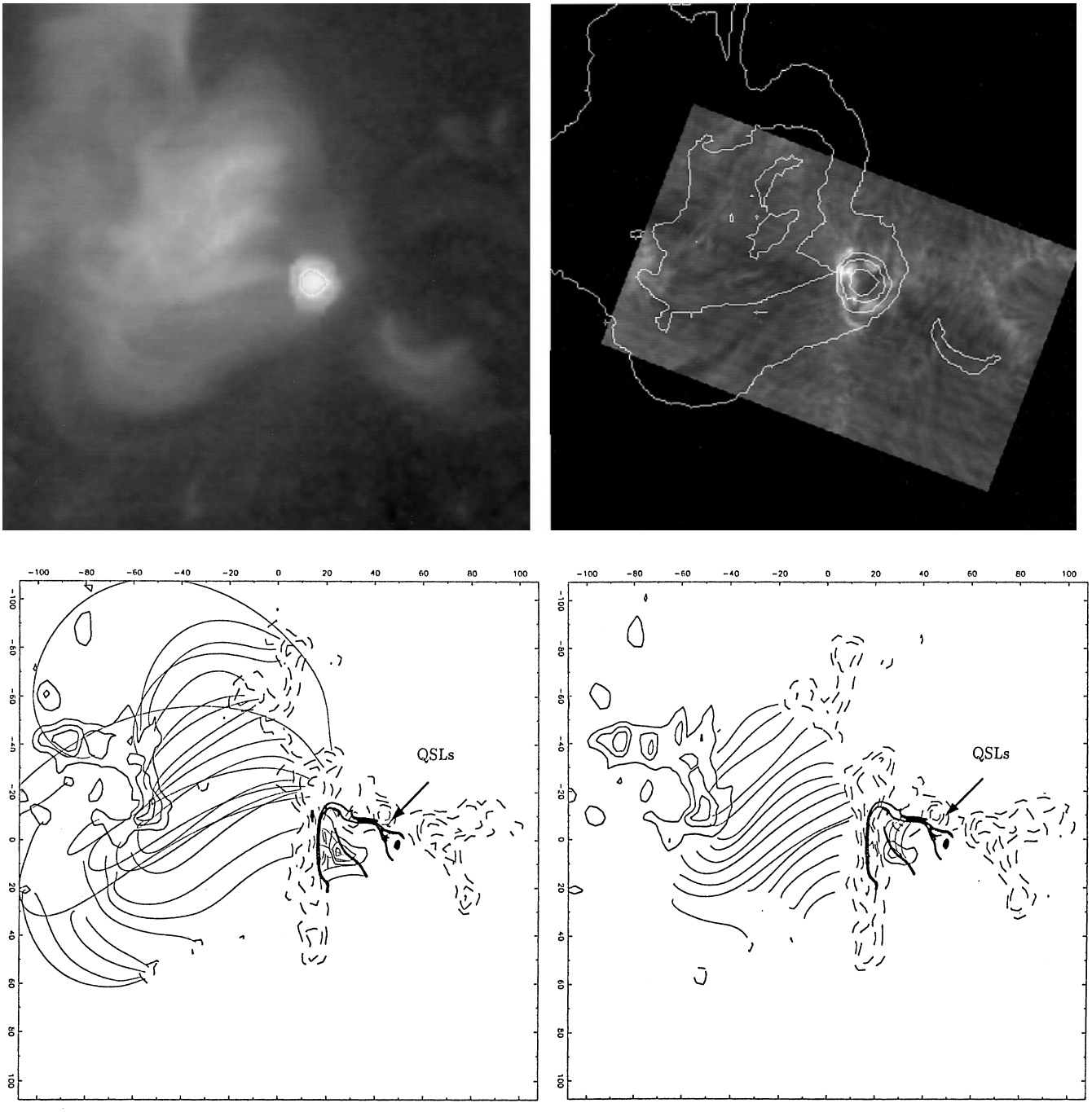

Fig. 7. Large-scale view comparison of the magnetic connections obtained with an extrapolation of the Kitt Peak magnetogram at 17:22 UT with observations. (a) X-ray observations and (b) corresponding magnetic field lines. (c) Hα observation (956 $\times$ 559 pixels of 0.225 arc sec^2) with X-ray contours and (d) corresponding magnetic field lines. In both figures, the QSLs related to the flares are shown by thick lines at the base of the configuration (isocontour N = 20). The isocontour levels of B_l (longitudinal magnetic field) are $\pm$60, 140 and 600 G.

diverge and have their other footpoints far from one another (B_1 is far from B_2). The locations where $N(x, y)$ takes its highest values define the field fines involved in the QSLs. By following these lines we can locate the coronal portion of the QSLs. We refer the reader to Priest & Démoulin (1995) and Démoulin et al. (1996) for a discussion of the properties of $N(x, y)$ and of the basic characteristics of QSLs.

The width of the QSL, δ, is defined at the half-height of the function N. Its value can be far smaller than the magnetogram resolution, but because δ is determined by the magnetic field of the whole region, the numerical grid needs only to be fine

enough to calculate the field line tying correctly (within the limits of the magnetic data and extrapolation). This point is justified in Démoulin et al. (1997).

3.3. Identification of the field lines implied in the flares

Some preliminary results of these computations have been presented in Schmieder et al. (1997b) and in Aulanier et al. (1997). The first step of this study is to find the average shear in the active region. In order to do so, we extrapolate the photospheric field with a given α, and we draw a number of field lines. As the largest computed field lines are more affected by shear, we compare them with the large loops observed in X-rays and Hα. We only draw the field lines we are interested in, and by making some variations on the a value, which is a free parameter in our extrapolation code, we finally get a good match between the high altitude X-ray loops, the lower ones appearmg in Hα, and the computed field lines (see Fig. 7). This value is $\alpha = 1.310^{-2} Mm^{-1}$.

We first focus on the field linkage around the flaring site, and we only draw the QSLs at this place. The feet of these QSLs are shown in Fig. 8 with an isocontour value of $N = 20$. We notice that some of them have the same shape as the bright Hα ribbons, at the same place where the X-ray emission is observed by SXT (see Fig. 5). The presence of QSLs at this particular place may explain the location of the X-ray and the Hα brightenings by magnetic reconnection. In order to confirm this hypothesis, we focus on this part of AR 7806, and we identify four kinds of field lines implied in the magnetic reconnection, and look for their observed signatures. The model is static and does not take into account an MHD evolution. Nevertheless, the model allows us to identify the field lines involved before (see Fig. 8 a,c) and after the reconnection (see Fig. 8 b,d). We show next that they represent the AFS, the C-shaped X-ray loop, the fishbone seen in X-ray during the flares, and some other ones too faint to be observed by SXT.

From the MSDP intensity and velocity data, we identify the field lines that correspond to the AFS (see Fig. 8 a,c). They interconnect the central QSL (QSL2) with the right one (QSL3). As the AFS has been observed to be rising into the corona during the flare, we suppose that its field lines interact with higher pre-existing loops. These are not observed by SXT because they very probably have a usual coronal temperature which is too low for Yohkoh/SXT. So we have to find these loops by the extrapolation.

We find that the C-shaped X-ray loop is composed of a series of magnetic loops which are anchored on the East side of the central QSL foot (QSL2) and on the West side of the left one (QSL1) (see Fig. 8 b,d). This is an important point, because it suggests that, in fact, some of the seemingly simple loops observed by SXT may represent an unresolved arcade. So we need magnetic observations at high resolution when we want to understand small scale X-ray features. The association of the C-shaped X-ray loop and AFS with field lines near QSLs, together with QSL properties, leads us to believe that the original pre-existing loops have their footpoints on the left side of QSL1 (see Fig. 8 a,c).

We finally locate the fourth kind of field lines associated with the QSLs as the ones starting on the north side of QSL3 (see Fig. 8 b,d). We can only identify the low altitude part of them as we do for the large pre-existing loops. They are nearly spatially coincident in vertical projection with the fishbone X-ray loops observed in the development of the first flare. Together with the magnetic loops associated with the C-shaped X-ray loop, they represent the magnetic field lines formed by reconnection of the emerging AFS with the pre-existing coronal loops (see Fig. 8).

This kind of field-line pattern has already been shown in theoretical flare configurations (see Démoulin et al. 1996), and observed ones (see Mandrini et al. 1996; Démoulin et al. 1997). The main difference here is that two sets of field lines look open. Our calculations show that even for a box 10^3 Mm high, these field lines do not close in the photosphere. However we do not know if these field lines are open or not to the interplanetary space for the following reasons: We have emphasized previously that large-scale harmonics given by the extrapolation method were very affected by small shear variations and these field lines are really very large. The average shear that we have found for this region is much approximated, so the behaviour of these loops is not well defined. Furthermore, we recently found that an active region could have a differential shear with height (see Schmieder et al. 1996b). This means that these large loops are not necessarily submitted to the same shear as the loops in the flaring site. The last reason is simply due to the geometry of the Sun: we cannot increase the height of the computation box infinitly, because higher up, the curvature of the Sun can not be neglected any more (Gary and Hagyard 1990 have shown that the computation error due to a flat magnetogram extrapolation is about 2 Mm for a 100 Mm structure located at 40° from the solar disk center). So we can only describe the shape of the low altitude field lines with our extrapolation code.

Finally, are the X-ray loops seen at the eastern part of the flaring region, magnetically linked to the flaring region? The magnetic extrapolation confirms what was guessed from the observations (see the last two paragraphs of Sect. 2.2); we do not find any magnetic field line starting at the flarerelated QSL, which can be interpreted as the eastern arcade of X-ray loops. Rather these loops can only be interpreted by field lines starting to the far East of the leading negative region (see Fig. 7), but without a direct magnetic link to the flaring loops. Their brightness may be due to a secondary process triggered by the flare (such as MHD waves coming from the flaring region). For these X-ray loops observed to the northeast of the arcade of X-ray loops, we have no counterpart for them in the extrapolation. However, it is note worthly that they are located close to the limb where we have no useful information on the vertical photospheric field.

3.4. Where does magnetic reconnection occur?

In order to understand why the flares occured at the location they did, we study the width δ of the QSLs involved in the process. A

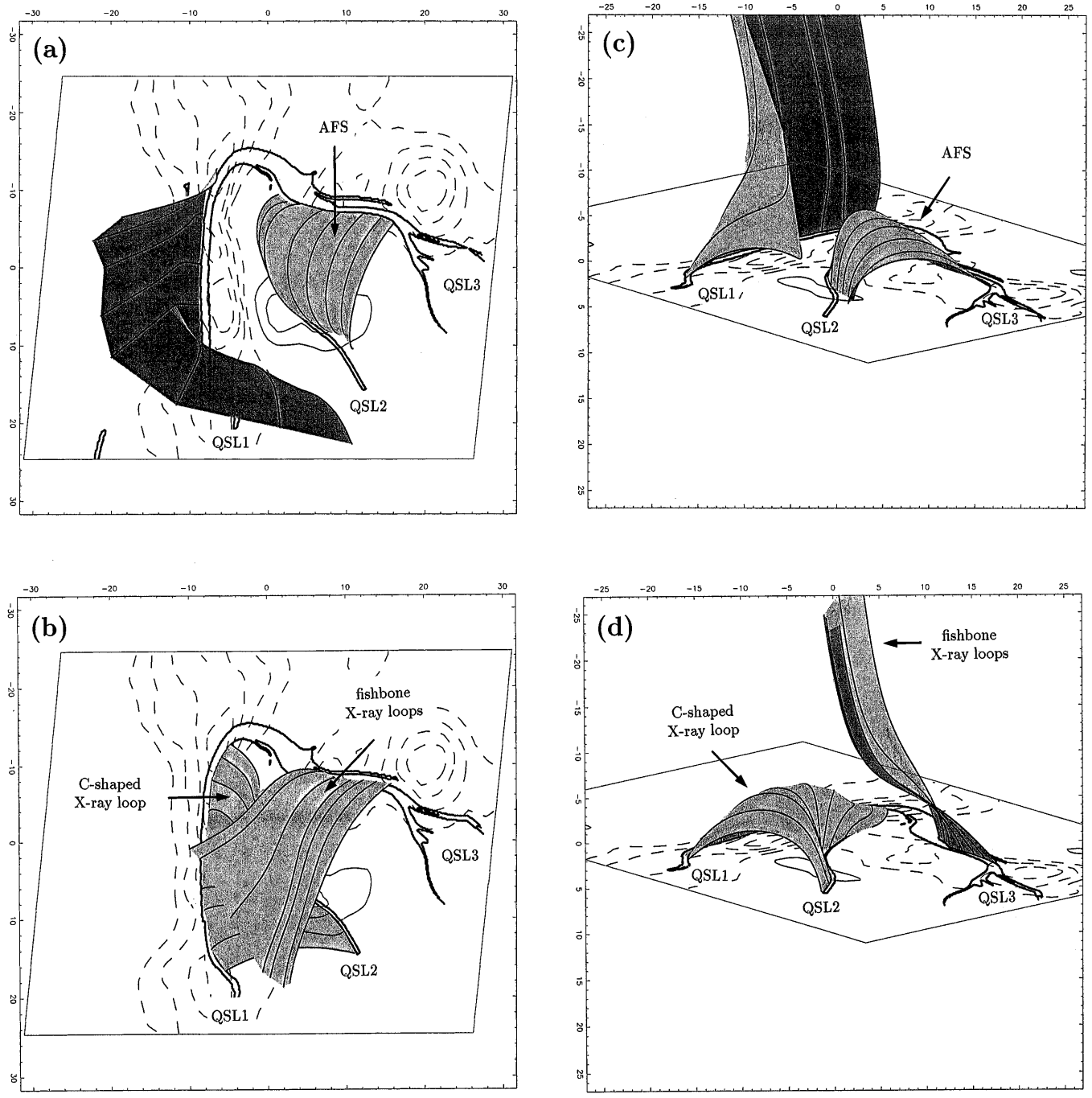

Fig. 8. Local view of the QSLs and field lines implied in the flares. The QSLs are only shown by isocontours of the function $N(x, y) = 20$ at the base of the configuration (thick lines). The four kinds of field lines implied in the reconnection are added on the sides of QSLs. **a,c** correspond to field lines before reconnection; **b,d** to field lines after reconnection. **a,b** are as seen from above; **c,d,** are side views. The AFS is localized at the closed field lines in **a,c** and the C-shaped X-ray loop at closed ones in **b,d**; the fishbone loops represent the open lines on **d**. Only these loops have observational signatures in Hα and in X-rays.

very thin width is required to have a break-down of ideal MHD for the coronal conditions (high magnetic Reynolds number). This requires also large N values because the local maximum N is proportional to $1/\delta$ (Démoulin et al. 1996). We focus on the photospheric feet of the QSLs because the photospheric (and sub-photospheric) evolution is the driving mechanism of the coronal field evolution. There are two kinds of QSL feet: the ones at the center (QSL2) and the ones which are located at the footpoints of the large loops (QSL1 and QSL3).

First, we focus on QSLs 1 and 3. They are located at the footpoints of large open computed field lines, so they behave like separatrices. In fact, we have shown previously (see Mandrini et al. 1996) that the evaluation of the width is limited, because of the numerical resolution. So we can only give upper limits for their width: $\delta(QSL1) \leq 25$ m and $\delta(QSL3) \leq 300$ m. They are so small that we can easily check that ideal MHD can break down at these places.

Then, we study QSL2, which lies between the AFS and the C-shaped X-ray loop. Its behaviour changes as we follow it from the North to the South. In fact, we can divide it into three regions: the upper one (North of the strong positive magnetic region), the middle one (on the strong magnetic flux), and the lower one (South of the strong positive magnetic region). Only the upper part of QSL2 is limited by the resolution, though we can find approximate values of δ for the other parts of it. We find that QSL2 is very thin in its upper and lower parts. Here, it behaves like a separatrice, where reconnection can take place.

$$\delta(QSL2)_{\text{upper}} \leq 1\,m \tag{2}$$

$$\delta(QSL2)_{\text{middle}} \simeq 10^4\,m \tag{3}$$

$$\delta(QSL2)_{\text{lower}} \simeq 100\,m \tag{4}$$

A complete 3-D MHD model of the emergence of the observed AFS in the corona is far from our present possibilities. Even supposing a quasi-static evolution, we know that intense electric-current densities are formed in the QSLs (Démoulin et al. 1996) but we are not able to compute their distribution in the coronal field, so we just make a crude attempt below to see if 3-D reconnection can effectively occur there. A quasi-static evolution is no longer possible when the magnetic field lines are forced by the boundary motions to move faster than the typical coronal Alfvén velocity. This can happen at the QSL location where photospheric motions are typically amplified by a factor N (Priest and Démoulin 1995, see also Lothian and Browning 1996). Let us evaluate the typical velocities involved within the linear force-free extrapolation with the simple relation: $v_{f.l.} \simeq N(x,y)v_{ph}$, where v_{ph} is the typical photospheric speed. We used a value of $v_{ph} = O.1\,km.s^{-1}$ and found:

$$v_{f.l.}(QSL2)_{\text{upper}} \geq 3.10^5\,km.s^{-1} \tag{5}$$

$$v_{f.l.}(QSL2)_{\text{middle}} \simeq 70\,km.s^{-1} \tag{6}$$

$$v_{f.l.}(QSL2)_{\text{lower}} \simeq 2000\,km.s^{-1} \tag{7}$$

Priest and Démoulin (1995) have suggested that at the location of a QSL, ideal MHD breaks down if $v_{f,l.} \geq v_{Alfven}$, and reconnection can take place. We give an evaluation of Alfvén speed at each part of QSL2.

$$v_{Alfven} = 2.8\ 10^6 B n^{-0.5} \tag{8}$$

where v_{Alfven} is in $[km.s^{-1}]$, n the electronic density in $[cm^{-3}]$ and the magnetic field magnitude B in $[G]$. We use the values of B given by the magnetogram, and the range of values for the electronic density we measured, which is reported in Table 2: For the C-shaped X-ray loop, we find $10^{10}cm^{-3} \leq n \leq 6.10^{10}cm^{-3}$.

$$300\,km.s^{-1} \leq v_{Alfven}(QSL2)_{\text{upper}} \leq 800\,km.s^{-1} \tag{9}$$

$$2400\,km.s^{-1} \leq v_{Alfven}(QSL2)_{\text{middle}} \leq 6000\,km.s^{-1} \tag{10}$$

$$300\,km.s^{-1} \leq v_{Alfven}(QSL2)_{\text{lower}} \leq 800\,km.s^{-1} \tag{11}$$

Then, with a linear force-free field extrapolation, reconnection seems to be possible directly at the Northern and the Southern part of QSL2. This means that we would have, in fact, two places where field lines are directly reconnected. We have an observational counterpart of that. The fishbone X-ray loops (oriented NW-SE) superposed on the C-shaped loop, are composed of two faint regions. They probably represent the base of the field lines of the large post-flare loops. They match quite well with the places where post-flare loops are likely to be formed by reconnecting some AFS field lines, at the north of QSL3 (see Fig. 8 b,d). The footpoints of these loops are located near two strong magnetic field negative polarities. At the middle part of QSL2, reconnection cannot occur spontaneously. A current layer is likely to be formed first, until a threshold is reached (see the discussion in Mandrini et al. 1996). Then, reconnection can occur. The absence of significant reconnection at the beginning of the interaction between the emerging and coronal fields may be a basic ingredient for the impulsive energy release in flares because even in the case of the emergence of a twisted flux tube the stored energy cannot be released without the presence of small scales.

This interpretation confirms our first analysis of the reconnection given in Sect. 3.3, but it gives some new details. With the emerging flux appearing in an old active region, an AFS is formed. Its field lines join QSL2 and QSL3. As they rise into the corona, its Northern and southem field lines start to reconnects with long pre-existing ones. But the center ones do not reconnect so easily, because at their footpoints QSL2 is not thin enough. The following interpretation can only be guessed from the known physical behaviour of the plasma in the corona. First, these field lines form a current sheet between themselves and the large pre-existing ones, and when this sheet is thin enough, reconnection can occur. This is not done continuously, because the relaxation of a non uniform current sheet is not continuous. As the AFS field lines reconnect with large loops, some small scale field lines are created between QSL1 and QSL2. The plasma is heated there, as it gets a lot of energy from the reconnection process. A cartoon of the whole process is given in Fig. 9. As the flare goes on, the magnetic region gradually loses

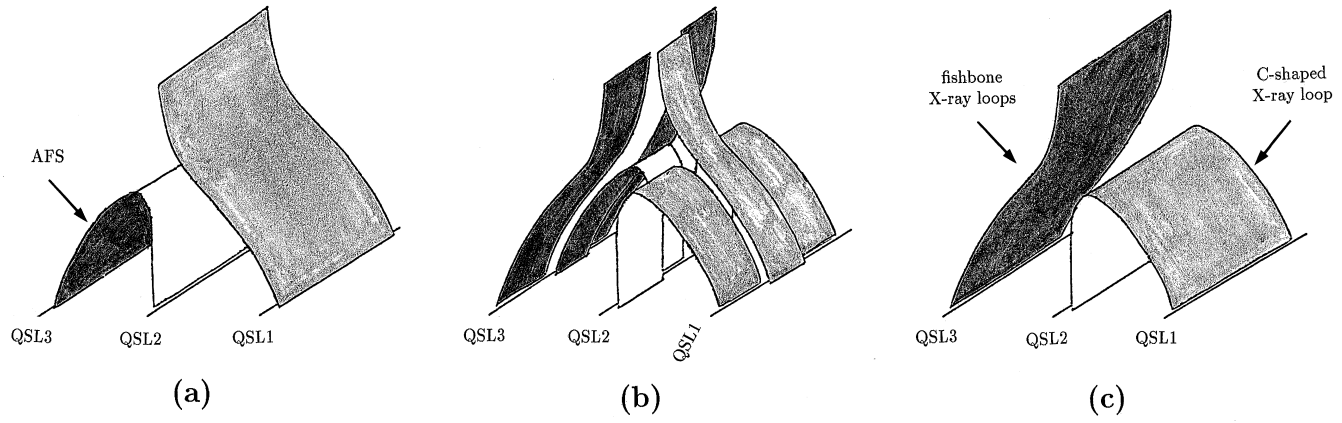

Fig. 9. Sketch of the reconnection process. **a** is the initial state. In **b** the field lines from the AFS, located at the ends of QSL2, reconncct directly. But the ones located at the middle part of QSL2 do not reconnect directly; a current sheet is likely to be formed between them and the open pre-existing loops, before they finally reconnect in **c**.

energy by Joule heating, and it slowly evolves towards a potential topology. This evolution probably creates MHD waves, that induce the brightening of large loops far to the East of the active region.

4. Conclusion

Solar events have signatures throughout the entire solar atmosphere, from the photosphere to the corona. To be able to understand an event, especially a small one, multi-wavelength observations represent a necessary tool. In this paper, we clearly illustrated this fact, with the study of two small, homologuous flares. The soft X-ray telescope abord Yohkoh provides us with very valuable information (location, density, temperature...) on the heated plasma, that is, on the coronal consequences of the energy release, but it is not sufficient alone to give hints on the origin of the flares. Moreover, for the case of compact flares, one has to remember that the size of the loops involved might be of the order of or under the spatial resolution of the telescope. Hα observations, instead, point out the origin of the flares: the emergence of new magnetic structures seen as an arch filament system. The magnetic data confirm this emergence, and permit computation of the coronal magnetic field. The eastern part of what we called the C-shaped X-ray loop (Sect. 2.3) was in fact understood as a series of small loops, with a nearly orthogonal direction to the loop-shape suggested directly by the X-rays. These loops join the two parallel Hα ribbons. The fishbone X-ray loops are the feet part of another set of reconnected field lines.

Combining all the observations and the modeling of the coronal field we reach the following flaring scenario. A small magnetic bipole (P2-N2) emerged in the leading part of AR 7608 (N1). This forced magnetic reconnection between the emerging flux and the large scale pre-existing coronal field. Reconnected loops are formed by an arcade of small loops (giving the eastern part of the C-shaped X-ray loop) and long loops (giving the west of the C-shaped X-ray loop and later on the fishbone X-ray loops). In fact only the lower part of the long reconnected loop can be filled with dense plasma, so that only the west-leg is observed. The long reconnected loops need more evaporate chromospheric material to fill them than for the short reconnected loops so at first we see a stronger X-ray emission in the eastern part of the C-shaped loop then, later on, the fishbone X-ray loops brighten.

The observations together with the model show that the flares were induced by the emergence of new flux which impacts and reconnects with long pre-existing coronal loops. Thanks to an observation campaign between several instruments it has been possible to understand what would have otherwise appeared as peculiar flares (which cannot be put in a common category). We have shown that the field line extrapolations and Quasi-Separatrix Layers (QSL) computations are well advanced now so that they can provide a powerful tool to understand complex observations.

Acknowledgements. The authors thank Drs M. Karlicky for the radio data, G. Csepura for Debrecen observations, J.M. Malherbe for fruitful discussions, J. Lemen for being the chief observer in the Yohkoh campaign, Arnaud Masson for reducing the MSDP data, and Daniel Brown for his help for the improvement of the manuscript. The NSO/Kitt Peak magnetogram data used in the paper are produced cooperatively by NSF/NOAO, NASA, GSFC, and NOAA/SEL, courtesy Karen L. Harvey. Mees Solar Observatory is supported by NASA grant NAGW 1542 to the University of Hawaii.

References

Alissandrakis, C.E., 1981, A&A 100, 197
Aulanier, G., Démoulin P., Schmieder, B., van Driel-Gesztelyi, L., Roudier, T., Nitta, N., 1997, proceeding of the JOSO 1996 meeting, 51
Démoulin, P., Hénoux, J.C., Priest, E.R. and Mandrini, C.H., 1996, A&A 308, 643
Démoulin, P., Bagalá, L.G., Mandrini, C.H., Hénoux, J.C. and Rovira, M.G., 1997, A&A in press.
Doschek, G.A., Strong, K.T., Tsuneta, S., 1995, ApJ 440, 370
Forbes, T.G. and Malherbe, J.M., 1986, Solar Phys. 302, L67

Forbes, T.G. and Acton, L., 1996, ApJ 459, 330 1983, ApJ 265, 1056
Hara, H., Tsuncta, S., Lemen, J.R., Acton, L.W. and McTierman, J.M., 1992, *PASJ*, 44, L135
Harrison, P.J., Duvall, T. L. Jr., Harvey, J.W., Mahaffey, C.T., Schwitters, J.D. and Simmons, J.E., 1992, Solar Phys. 139, 211
Leka, K.D., Canfield, R.C., McClymont, A.N., and van Driel-Gesztelyi, L., 1996, ApJ 462, 547
Lothian, R.M., and Browning, P.K., 1996, Solar Phys. 161, 289
Mandrini C.H., Démoulin P., Van Driel-Gesztelyi, L., Schmieder, B., Cauzzi, C. and Hoftnann, A., 1996, Solar Phys. 168, 115
Mein, P., 1977, Solar Phys. 54, 45
Mein, P., Démoulin, P., Mein, N., Engvold, O., Molowny-Horas, R., Heinzel, P. & Gontikakis, C. 1996, A&A 305, 343
Mickey, D.L., Canfield, R.C., LaBonte, B.J., Leka, K.D., Waterson, M.F., and Weber, H.M., 1996, Solar Phys. in press.
Priest, E.R. and Démoulin, P., 1995, JGR 100, A12, 23443
Ruždjak, V., Zlobec, P., 1994, proceeding of the JOSO 1994 meeting, 188
Schmieder, B., Heinzel, P., van Driel-Gesztelyi, L., Lemen, J.R., 1996a, Solar Phys. 165, 303
Schmieder, B., Démoulin, P., Aulanier, G., Golub, L., 1996b, ApJ 467, 881
Schmieder, B., Malherbe, J.M., Mein, P., Mein, N., van Driel-Gesztelyi, L., Roudier, T., Nitta, N., Harra-Murnion, L.K., 1997a, *PASP*, Eds. B.Bentley, J.Mariska, vol 111, 43
Schmieder, B., Démoulin, P., Aulanier, G., Malherbe, J.M., van Driel-Gesztelyi, L., Mandrini, C.H., Roudier, T., Nitta, N., Harra-Murnion, L.K., 1997b, Advances in Space Research, in press.
Tsuneta, S., Acton, L., Bruner, M., Lemen, L., Brown, W., Caravalho, R., Catura, R., Freeland, S., Jurcevich, B., Morrison, M., Ogawara, Y., Hirayama, T., and Owens, J., 1991, Solar Phys. 136, 37
van Driel- Gesztelyi, L., Schmieder, B., Cauzzi, G., Mein, N., Hofmann, A., Nitta, N., Kurokawa, H., Mein, P., Staiger, J., 1996, Solar Phys. 163, 145

This article was processed by the author using Springer-Verlag LaTeX A&A style file *L-AA* version 3.